MISSING MASS SPECTROMETER FOR HEAVY MESONS

Proposal for an experiment

Bogdan Maglić and Giovanni Costa

CERN

Contents

30th May, 1963

* Prepared with the aid of G. Charpak

MISSING MASS SPECTROMETER FOR HEAVY MESONS

1. Purpose of the Experiment

We propose a detailed investigation of the mass spectrum of heavy mesons (multi-meson "resonances") in the region $1 < M < 3$ GeV. The purpose of the measurement would be to establish negative or positive evidence for the existence of resonant states in this, so far unexplored, mass range. Examples of multi-pion states that could be expected are the "heavy pion" with $J = 2^-$ and the "heavy rho", a meson with $J = 3^-$, both with $I = 1$. (See Appendix A.)

The proposed reaction is :

$$\pi^- + P \rightarrow P + X^- \qquad (1)$$

where the heavy meson decays :

$$X \rightarrow N\pi \qquad (1')$$

with $N = 2, 3 \ldots 5 \ldots 10 \ldots$.

Specification of the aims

The proposed measurement should be able to detect all mesonic states, X,

- of charge $Q = -1$, i.e. states of isotopic spin $I \geq 1$;
- in the mass range :

  $0.5 \leq M_X \leq 3.5$ GeV, (with the emphasis on the 1-3 GeV region) ;

- produced in peripheral collisions in the range of the momentum transfer given by :

  $0.2 < \Delta^2 < 1.6$ $(\text{GeV}/c)^2$;

- produced with a total cross-section $\sigma_x \geq 0.50$ mb ;

The measurement will have a mass resolution of $\Gamma_{exp} = 20$ MeV, so that

- it should be able to separate two peaks if they are more than 20 MeV apart ;
- it should determine the physical width of a state of any mass of $\Gamma \geq 20$ MeV of the state.

The maximum aims of the experiment* are :

- to determine the decay products of the state X, if found, i.e. whether these are pions or kaons or both ;
- into how many charged π mesons, charged K mesons and neutral K mesons new particle X decays. This might set a basis for a speculative spin parity assignment, or the lower limit to the spin, J_{min} (See Appendix D) ;
- to determine the mechanism responsible for the production of the X, if found. E.g. in not too unfavourable background conditions, the shapes of the distributions would be different for π and η exchange mechanisms (See Appendix C).

The expected by-products of the experiment are :

- cross-section for the ρ production in reaction (1),

---

* i.e. not essential to the main objective, which is to establish the existence of peaks in the missing mass spectrum.

between 5-7 GeV/c ;

- width Γ and the shape of the ρ ;
- evidence of the existence or non-existence of the ζ meson ;
- excitation function for the production of charged pions for each multiplicity, for incident pion momenta 5-14 GeV/c or N_π vs bombarding energy.

2. Method

Basic Method

With the fixed incident pion momentum, p_1, in the reaction :

$$\pi^- + P \rightarrow P + N\pi \ , \qquad (2)$$

a simultaneous measurement of two quantities: the outgoing proton momentum p_3 and the proton angle Θ_3 gives the missing mass of the proton, MM, which is equal to the effective mass of the N pions, $M_{N\pi}$,

$$(MM)^2 = M_{N\pi}^2 = (E_1 + m - E_3)^2 - p_1^2 - p_3^2 + p_1 p_3 \cos \Theta_3 \qquad (3)$$

For uncorrelated pions, the distribution in $M_{N\pi}$ is a smooth function with a broad maximum ; however, in N pions "resonate", the process becomes a two body one, Reaction (1), and a peak in the distribution will occur at a set of combinations of p_3 and Θ_3 (a mass M_x).

Novelties in our Application of the Method

We can show that, with any fixed p_1 and properly chosen kinematic conditions, the existence of Reaction (1) can be experimentally determined by measuring only one quantity: the angle Θ_3. The proton momentum p_3 does not have to be measured; it is sufficient to set (experimentally) the upper and the lower limits to the proton momenta. The existence of a discrete mass in Reactions (1) and (2) will manifest itself as a peak in the angular distribution of protons of all momenta in a given momentum band. The above statement is valid in the angular region about the maximum laboratory angle of the recoil proton, Θ_3^{max}, which is between 45° and 65°, depending on the M and p_1. This is the consequence of a property of the Jacobian, for cases in which $\beta_c > \beta_3°$ (See Appendix B).

In addition, the choice of the angular range around Θ_3^{max} has two other advantages:

- with the incident pion beam of a momentum in the range $6 < p_1 < 15$ GeV/c, the investigated protons will have a momentum $0.400 < p_3 < 1.1$ GeV/c or a kinetic energy $80 < T_3 < 500$ MeV, thus reducing the experiment to the low-energy one, as far as the proton detection is concerned.

- The proton background from reactions of the type:

$$\pi^- + P \rightarrow P^* + N\pi \quad \hookrightarrow P + \pi \qquad (4)$$

where N^* is any nucleon isobar, is kinematically limited to a cone given by $\Theta_3 \leq 40°$. Since we are to work in the range $\Theta_3 \geq 45°$, about 95% of the background from (4) is eliminated, and only Reaction (2) will contribute to the background.

3. Experimental Requirements

Experimental requirements needed to make observations as specified under paragraph 1, are listed in Table I.

Table I

Typical Resolution Needed to Identify a Mesonic State of Mass M = 2 GeV, Γ = 20 MeV

1 Parameter	2 Range of p_1, p_3 and Θ_3 min.	2 Range of p_1, p_3 and Θ_3 max.	3 Full width resol. expect.	5 Resolution function Γ_{exp} due to uncertainties in Col 3 (keeping the other two constant)	6 Proposed Instrument
p_1	6 GeV/c	12	$\frac{\Delta p_1}{p_1} = 1.5\%$	8 MeV	Counter hodoscopes
p_3	0.4 "	1.1	none, only upper cut-off has to be known to $\frac{\Delta p_3}{(p_3)_{max}} = 10\%$	5 MeV	Aluminium block to stop all protons below 1.1 GeV/c plus time-of-flight measurements.
Θ_3	45°	65°	$\Delta\Theta_3 = 12$ mrad*	12 MeV	3 thin-plate spark chambers; photographic and sonic data recording

Total Width Γ^{rms}_{exp} = 16 MeV

* Multiple scattering in target and spark chambers included.

4. Experimental setup

The experimental setup is shown in Figure 1. Beam hodoscope system $H_1 H_2 H_3$ serves to determine the pion momentum and the direction before scattering.

The first hodoscope, H_1, consists of five vertical counters, each 2 mm wide. The second and third hodoscopes, H_2 and H_3 consist of five vertical and three horizontal counters. The pulses from each counter from H_2 and H_3 are divided into two outputs, A and B. Outputs A go into the H_1-H_2-H_3 coincidence circuitry. Outputs B are fed into the data recording system.

The system H_1—H_2 is connected as fixed deflection selector*: the coincidences occur only if the pion passes through a fixed pair of counters; e.g. passage through counters 13 and 23 produces coincidence, while through 13-14 does not.

On the other hand, the passage of the pion between any counter in H_2 and any counter in H_3 produces coincidence.

The system is illustrated in Table II and Figure 2.

---

* suggested by G. Giacomelli

Table II

Beam hodoscope system

Hodoscope	Position	Consists of	Signal from each counter divided*	Plane in which the position is defined
H_1	5 m before C	5 x 2 mm wide counters	No; only A	horizontal only
H_2	4 m behind C	5 x 2 mm cs. 3 x 3.3mm "	Yes A, B	horizontal vertical
H_3	8 m behind H	5 x 2.5mm " 3 x 4.2mm "	Yes A, B	horizontal vertical

* A = To trigger logics
B = To data recording system, 16 binary numbers + event number.

Momentum resolution of the pion beam

If θ_0 is the angle of deflection of the pion beam through the magnetic spectrometer, the momentum resolution is :

$$\frac{\Delta p_1}{p_1} = \frac{\Delta \theta_0}{\theta_0}$$, with θ_0 = 100 mrad, in our conditions.

$\Delta \theta_0$ = The angular uncertainties in θ_0 , are listed in Table III

Table III

Angular Uncertainties $\Delta\vartheta_0$ in mrad

Cause	Beam section from - to	$\Delta\vartheta_0$-Maximum (p_1 = 5 GeV/c)	$\Delta\vartheta_0$-Minimum (p_1 = 12 GeV/c)
Finite size of counters	H_1 - C	$2\,\frac{2}{5000}$ = 0.56	0.56
"	H_2 - H_3	$\frac{1}{8000}(2.5+2)$ = 0.40	0.40
Mult. Scatt. in counters	H_1 - C	Total thickness 3 mm: 0.42	0.21
"	H_2 - H_3	Total thickness 12 mm: 0.84	0.42
Mult. Scatt. in 17 m helium bag	H_1 - to the front of the target	0.08	0.04
	Total:	$\Delta\theta_{0\,rms}^{max}$ = 1.27	$\Delta\theta_{0\,rms}^{min}$ = 0.83

Therefore:

$$\left(\frac{\Delta p_1}{p_1}\right)_{max} = \frac{1.27}{100} = 1.27\% \qquad \left(\frac{\Delta p_1}{p_1}\right)_{min} = \frac{0.83}{100} = 0.83\%$$

and we expect a momentum resolution in the limits:

$$0.8\% \leq \frac{\Delta p_1}{p_1} \leq 1.3\% .$$

Target

The liquid hydrogen target is 70 cm long, 20 cm wide, 30 cm deep. Beam hits the target off-centre with the centre of the beam

1.0 cm from the side wall of the target. Multiple scattering angle through the hydrogen:

For .400 GeV/c protons : 7 mrad
1.1 GeV/c protons : 2 mrad

Upper and lower limits to the proton momentum, p_3

We set the lower and the upper limit to p_3 by the range method.

Lower limit: Aluminium plate R 1 in Fig. 1, 2.5 cm thick in front of counter hodoscope P_1 - P_6 will stop all protons with $p_3 < 400$ MeV/c.

Upper limit: Block of Aluminium plates, R 2 in Fig. 1, 50 cm thick, in front of anticoincidence hodoscope $\bar{P}_1$ - $\bar{P}_3$ will stop all protons with $p_3 < 1.1$ GeV/c.

Each counter of the P_1 - P_6 hodoscope will have the output divided into three channels A, B and C. Pulses A is fed into the coincidence logics. Pulses B go into the data recording system and registers which counter went off. Pulses C are all added and connected to the travelling wave scope for measuring the time-of-flight

Proton Identification

Time of flight between H3 and C1-C5 counters

Proton Momentum p_3	β_3	Delay in 3 m
Min.: 0.400 GeV/c	0.39	26 nsec
Max.: 1.1 "	0.79	12 "

Minimum time of flight for acceptance : 13 nsec. This criterion eliminates recoil protons from the elastic scattering.

In addition to these timing conditions to satisfy our coincidence circuitry, we shall make a photographic record of the time-of-flight for each individual event, by using the travelling wave scope. The event number (no. of the trigger) is to be displayed on the picture as well. While this information is not essential to the concept of our experiment, it introduces a safety factor: if for some reason we decide that more information on the proton momentum is needed, than the mere fact that it was within the given limits $0.4 < P < 1.1$ GeV/c, we can divide the events into narrow momentum bands of 200 MeV/c ($\Delta\tau \cong 4$ nsec).

Determination of the Proton Direction

Thin plate picture fram spark chambers, 3 each.

Both photographic and sonic systems will be used with these three spark chambers. Two gaps of each chamber will have four microphones/gap on the sides not used for the optical path, like this:

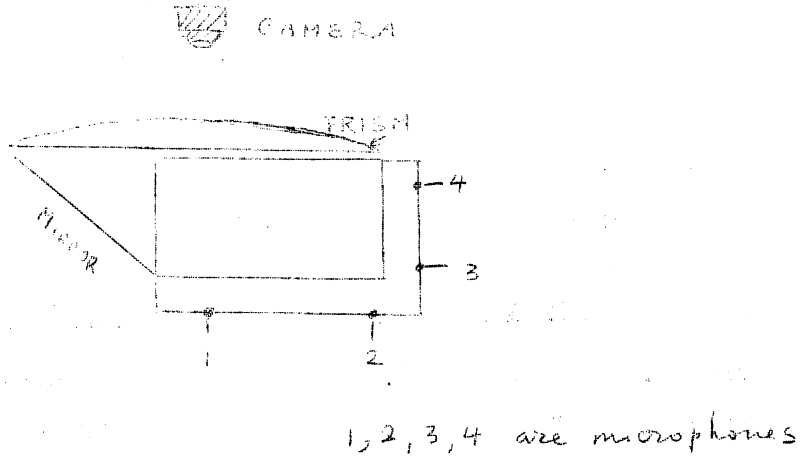

1, 2, 3, 4 are microphones

This requires a total of twenty-four microphones; the coordinates will be recorded from twenty-four scalers onto the punched paper tape.

The sonic system will make it possible to have an on-line data reduction sampling operation. We expect to obtain histograms of our angular distributions (= missing mass spectra) every 6 - 8 hours. On the basis of these, we can optimize our parameters in the course of the experiment; we shall probably be able to "hunt" the peaks in a controlled manner.

However, we estimate that between 10% and 20% of the triggers will have only one particle track in the spark chambers and sufficiently clean conditions (absence of spurious sparks) to allow for extracting the sonic information. Therefore, we chose the photographic system as the major means for the data storage:

a) spurious sparks or edge tracks are easily eliminated by scanning;

b) in case of two tracks through the chambers, the information on the no. of counter in P_1 - P_6 hodoscope will be able to indicate which one has produced the trigger.

The photographic data are analyzed after the experiment.

Table IV

Uncertainties in the proton direction due to the multiple scattering in spark chamber plates

Chamber	Dimensions	No. of gaps	Total thickness	Mult.scatt. ang. (mrad) for p_3 = 600 MeV/c
1	80 x 25 cm^2	5	0.0200 cm	3.75
2	110 x 50 cm^2	3	0.0100	2.65
3	140 x 80 cm^2	5	0.020	3.75
			Total	5.9 mrad

Table V

Angular uncertainty in determination of the proton angle Θ_3

Cause		$\Delta\Theta_3$ max	$\Delta\Theta_3$ min
Initial pion direction	finite size	0.40 mrad	0.40 mrad
	mtpl scattering in counters	0.84	0.42
	mtpl scattering in He-bag	0.04	0.02
Mult. scattering in target		7.00	2.00
spark position		0.5	0.5
mult. sc. in $S_1S_2S_3$		5.9	5.9
Total uncertainty:		$\Delta\Theta^{max}_{rms}$ = 9.3 mrad	$\Delta\Theta^{min}_{rms}$ = 6.25

This compares favourably with the expected width of the peak in angular distribution, which is 14-18 mrad.

Vertex Chamber

The discharge halogene chamber will be placed right behind the target, at 3^o in the direction of the beam.

The chamber will be triggered every time the chambers $S_1S_2S_3$

are triggered. If a peak is found in the proton distribution, the event numbers corresponding to the events in the peak will be listed; only these pictures in the vertex chambers will be scanned. It is hoped that the scanning will establish the decay modes of the new resonance; i.e. the number of charged pion or kaons or K^{o}'s.

Two possibilities, now under consideration, are listed in Table VI.

Table VI

Discharge halogene chamber as Vertex chamber

(See Appendix D)

Chamber	Magn. field	Size cm^3	State	Angle Horiz.	Angle Vert.	% of decay products to be lost	Analysis, if a peak is found
Small	Yes 13 kG	50x50x40	Constructed and tested	20^{o}	10^{o}	50-60	Positive, negative and V's are counted, only in photos correlated to the peak. The vertex is reconstructed and compared with the proton vertex (should be the same).
Large	No	100x70x70	Being constructed	80^{o}	20^{o}	10-20	Count charged particles and V's. Accept only events with odd number of charged tracks. Reconstruct vertex and with the proton vertex (same).

5. PROCEDURE, YIELD AND MACHINE TIME NEEDED

Experimental procedure

Throughout all runs, from 5 to 12 GeV/c, we cover only one area in the cos θ_3 vs P_3 plane, the area of maximum sensitivity for the detection of a peak in the missing mass distribution. (Fig. B1, B2) Experimentally this means:

a) angular region is always $45^\circ < \theta_3 < 65^\circ$; this covers the mass band 1 GeV wide.

b) momentum range is kept constant, $0.42 \leq P_3 \leq 1.1$ GeV/c by means of absorbers R1 and R2 as well as the time-of-flight limits.

We bring higher and higher masses into the sensitive area by increasing the pion momenta in steps of 1 GeV/c. Since our angular range covers as much as $\Delta M = 1$ GeV at each pion momentum, we could cover the desired region $M_x = 1 - 3$ GeV in only three runs. However, too large steps can lead to an omission of some states: the production mechanism or interference effects in the final state may favour some bombarding energies over others. Also, the non-resonant background changes its shape at various pion energies.

Therefore, we chose to make a lot of overlaps and plan to cover the desired mass range roughly like this:

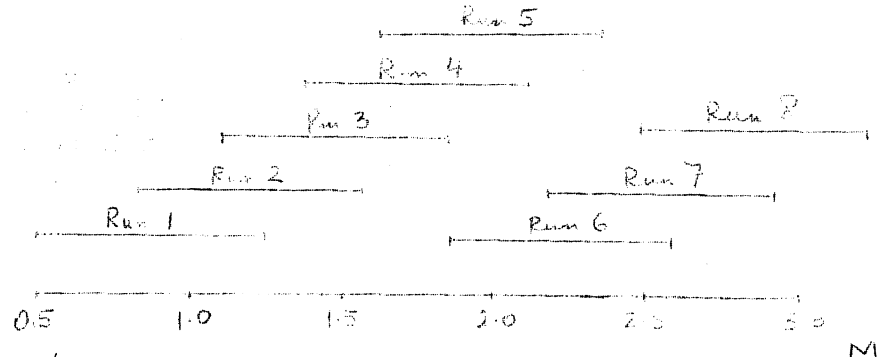

(Further procedure to take place <u>if</u> a peak is found, is described under "Vertex chamber".

<u>Triggering Rate</u>

Sketch of the target-detector geometry

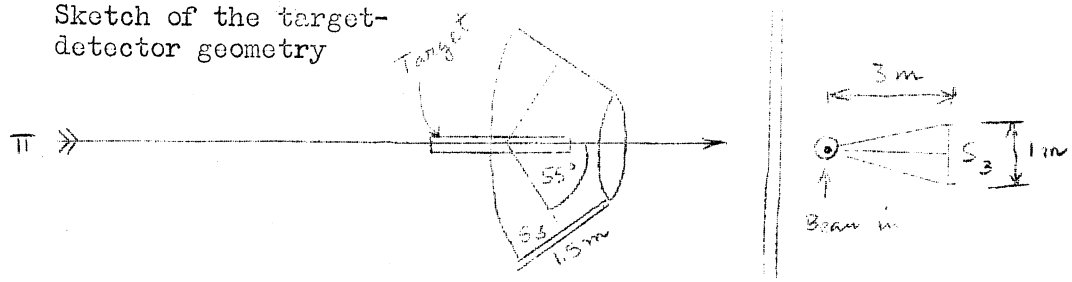

Yield : $n = \ell \cdot \sigma_{tot} \cdot f \cdot \frac{\Delta\varphi}{360}$ protons/pion

ℓ = length of the target

σ = total cross section for X production

$f = \frac{\Delta\sigma}{\Delta\Theta_3}$ = fraction of σ in the region Θ_3 of the Jacobian peak

$\Delta\varphi$ = azymuthal angle.

$\ell = 70$ cm $\quad \sigma = 1$ mb $\quad \ell\sigma = \frac{1}{500}$

$\frac{\Delta\sigma}{\Delta\Theta} = 10\% \quad \frac{\Delta\varphi}{360} = \frac{1}{20} = 0.05$

$n = \frac{1}{500} \quad \frac{1}{10} \quad \frac{1}{20} = \frac{1}{500} \quad \frac{1}{200} = 1 \times 10^{-5}$ "real events"

or : 1 mb corresponds to 1 proton into our detection system, with $10^5 \pi$ / burst.

In addition to "real events", we shall have background protons, whose estimated intensity is listed in Table VII.

Table VII

Background reactions

No.	Background Reaction	σ_{tot} (Guesstimated)	f = Fraction of σ_{tot} to enter our system
1	$\pi^- + P \rightarrow P + \pi^-$	9 mb	f = 0. Protons too high momentum will be rejected both by time of flight and by range antico counter.
2	$\pi + P \rightarrow P^* + \pi$ $\rightarrow P^* + N\pi$	9 mb	f = 0. The maximum angle for proton beam from $P^* \rightarrow P + \pi$ is 35^o, while we look only at $\theta_3 > 45^o$.
4	$\pi^- + P \rightarrow P + N\pi$	8 mb	$f^{max} = 0.5$. We know average $\bar{N} = 6$, charged or neutral. The effective mass distribution for high multiplicities is known to be peaked toward high masses, while we work in lower half of the spectrum.
5	$K^- + P \rightarrow P + K + N\pi$	?	The K^- contamination is 1%. We are not going to worry about this.

It follows that the maximum contribution from the background is 4.0 mb. Thus we can expect to work in ratio $= \frac{\text{signal}}{\text{noise}} = \frac{1}{4}$. Since the yield for "real" events was estimated 1×10^{-5} sec, the total yield or the total trigger rate now becomes 5×10^{-5} triggers/pion.

We need a beam intensity of 2×10^4/burst, in order to get 1 trigger/burst.

The signal-to-background ratio 1 : 4 requires statistics of 3% in order to clearly separate the signal, or 1000 events per "bin" (= plotting interval). We would like 30 bins at each energy, i.e. 30,000 triggers in each missing mass distribution (each run).

Run	p_π GeV/c	No. of good triggers
1	5	3×10^4
2	6	3 "
3	7	3 "
4	8	3 "
5	9	3 "
6	10	3 "
7	11	3 "
8	12	3 "
		2.4×10^5 good triggers

Taking a safety factor of 2, we require a total of 500,000 triggers = 4 weeks of machine time = 76 shifts.

6. DATA REDUCTION

The outline of the data reduction system is schematically given in Fig. 3. The coincidence logics is not shown in this figure (see Figs. 1 and 2).

On-line data

The horizontal (5 binary numbers) and vertical (3 binary numbers) positioning of the pion in each of the two hodoscopes, H_2 and H_3, gives the initial pion momentum p_1 and its direction before scattering.

The position of the proton through each of the spark chambers, S_1, S_2 and S_3 is given (overdetermined) by 24 microphones, connected to the scalers. One scaler is for the trigger number.

The position of the proton in hodoscope P_1 - P_5 has to be correlated to the proton direction through the chambers S_1 - S_3.

The magnetic tape units takes 21 binary numbers from counters and 25 words of 13 binary bits each from scalers.

The tape is taken to IBM 7090 computer, which evaluates: (1) p_1 for all triggers and (2) Θ_3 for those triggers in which spark chamber information was sufficiently clean to allow for sonic reconstruction of the proton direction, 10 to 20% of the total number of triggers. The programme rejects the events with double sparks.

Histograms of MM-spectra are to be plotted by such a programme in the course of the experiment.

Off-line data

Camera 1 gives spark positions in S_1 - S_2 - S_3 and the proton direction. Trigger number appears on each photograph. Measuring is to be done on HPD. Correlation with the information from H_2 - H_3 and P_1 - P_5 is done by another programme.

Camera 2. The film is used only if there is a need to make detailed analysis of P_3 (time-of-flight) and to split the data according to P_3 intervals.

Camera 3. Data from vertex chamber are used only if a peak is found. (See pages 12 and 30)

Appendix A

Experimental situation with mesons

There have been seven heavy mesonic states reported until now. Their mass spectrum is given in Figure A1.

Region Below 1 GeV

With exception of η', the eight-fold way predictions seem to be almost fulfilled (Table A1).

TABLE AI

	J^P / I	0^-	1^-
Isospin triplet	1	π	ϱ
	$\frac{1}{2}$	K	K*
	0	η	ω
Isospin singlet	0	$\eta' = ?$	$\omega' = \varphi$

The detail properties, such as the physical widths, for most of these states have not been completely investigated.

Region Above 1 GeV: f Meson

However, the existence of the f-Meson with $J=2^+$ makes the 8-fold scheme insufficient. There are several many-fold way schemes; the details of these are beyond the scope of this Appendix. Their only importance to the experimental approach is : the schemes can accommodate a number of mesonic states of J=2, 3, etc.

Unexlpored Region Above 1 GeV

The mass-spectrum in Fig. A1 shows that the region above M = 1 GeV has not been explored. The reasons for this are purely experimental, because, for the states of heavy mass the following difficulties arise:

a) the threshold for their production requires higher pion energies (5-12 GeV) where the average pion multiplicity is about 6 (4 charged, 2 neutrals); thus the kinematic fitting becomes very difficult or, when there is more than neutral, impossible. Distinction between charged K and pions almost impossible too.

b) 1 < M < 3 GeV. are likely to decay into a large number of pions, N = 3 or 4; the number of combinations of charged pions needed to evaluate the effective mass becomes prohibitive (e.g. 6π can form 15 pairs, 20 triplets, 15 quadruplets etc.)

It is felt that the proposed missing mass technique, at least in part, circumvents these difficulties.

Possible Heavy Mesonic States

Without any of the schemes or theories, only by writing down possible combinations of quantum numbers, one can list the possible mesonic states (Tables AII and AIII).

There is no a priory reason why should not any of the mesons, for which there is room in Tables AI and AII, exist. These states may be thought of as either many-π resonances or η-π, ρ-π, ω-π, ω-ρ etc. resonances. The absence of theories of higher mesonic states should not prevent the experimental inquiries. If future experiments show that for some combinations of quantum numbers there are no corresponding physical states, a challenging theoretical task would be to explain why is this so; thus the establishing of the absence of some mesons may be in some cases a more important experimental finding than the establishing of their existence.

Table A II

Possible mesonic states of odd parity (based on no theory)

I \ J^{PG}	PS 0^{-+}	PS 0^{--}	V 1^{-+}	V 1^{--}	T 2^{-+}	T 2^{--}	T 3^{-+}	T 3^{--}
0	η 550 <15			ω 785 <15				
1/2	K 495	K_1 10^{-16} K_2 10^{-14}	K* 885	66				
1		π 10^{-14} sec 140	ϱ 750	80				
3/2								
2								

Table A III

Possible mesonic states of even parity (no theory)

I \ J^{PG}	S 0^{++}	S 0^{+-}	AV 1^{++}	AV 1^{+-}	T 2^{++}	T 2^{+-}	T 3^{++}	T 3^{+-}
0	ABC 325	30			f 1250	50		
1/2	725	M ? <20						
1								
3/2								
2								

Notation:

Particle
Mass Mev $\quad$ P_{Mev}

S = SCALAR

PS = PSEUDO-SCALAR

V = VECTOR

T = TENSOR

NOTE: G IS NOT DEFINED WHEN I IS HALF-INTEGER OR WHEN STRANGENESS $\neq 0$.

This is particularly true in the view of the Regge-pole approach to elementary particles; its states with J^P reoccur at a higher (and definite) mass and $J' = (J+2)^P$. For example:

J^P	Particle	Reoccurrence J'^P	Particle	Decay
0^+	Vacuum	2^+	f	$\pi^+ + \pi^-$
0^-	π	2^-	?	$\rho + \pi$
1^-	ρ	3^-	?	$\omega + \rho$; $\omega + \pi$
1^-	ω	3^-	?	$\eta + \omega$

Positive or negative evidence for these states would be a critical test of the theory. Determination of their masses would show how valid is the assumption that the Regge trajectories are straight lines.

Appendix B

Kinematics of the reaction $\pi + P \to P + X$

The formula on which we base our kinematical considerations gives the mass of the X particle in terms of laboratory quantities:

$$(B\text{-}1) \qquad M^2 = (E_0 - E_3)^2 - (p_1^2 + p_3^2 - 2p_1 p_3 \cos\Theta_3)$$

where $E_0 = E_1 + m$, and E_1, p_1, E_3, p_3 are the energies and momenta of the incident pion and scattered nucleon, respectively.

In order to show how the determination of M is affected by the precision with which the quantities p_1, p_3, $\cos\Theta_3$ are measured, we report here the partial derivatives of M^2:

$$(B\text{-}2)\begin{cases} \frac{1}{2}\frac{\partial M^2}{\partial p_1} = -\beta_1 T_3 + p_3 \cos\Theta_3 \cong \frac{\Gamma^{p_1}_{exp}}{2}\frac{2M}{\Delta p_1} = \Gamma^{p_1}_{exp}\frac{M}{\Delta p_1} \\ \frac{1}{2}\frac{\partial M^2}{\partial p_3} = -\beta_3 E_0 + p_1 \cos\Theta_3 \cong \Gamma^{p_3}_{exp}\frac{M}{\Delta p_3} \\ \frac{1}{2}\frac{\partial M^2}{\partial(\cos\Theta_3)} = p_1 p_3 \cong \Gamma^{\Theta_3}_{exp}\frac{M}{\sin\Theta_3\,\Delta\Theta_3} \end{cases}$$

We remark that at high energy $\left(\beta_1 = \frac{p_1}{E_1} \simeq 1\right)$, $\frac{\partial M^2}{\partial p_1}$ does not depend on p_1. On the other hand, the choice of the values of p_1 affects the values of the other two derivatives, and therefore the precision which can be obtained in the determination of M. We believe that we can define M within a full "width" $\Gamma \cong 30$ MeV.

From (1) one obtains

$$(B\text{-}3) \qquad \cos\Theta_3 = \frac{M^2 - \mu^2 + 2E_0 T_3}{2p_1 p_3}$$

In Figs. B1 and B2 some graphs for $\cos\Theta_3$ are drawn as function of p_3, for different values of M, and for p_1 = 6 GeV/c and 8 GeV/c. With each value of M, we consider also the value $M + 1^7$.

One sees that all the curves have a minimum, which corresponds, for given p_1 and M, to the maximum angle Θ_3^{max} which is allowed in the laboratory system. The maximum for Θ_3 occurs at the energy of the recoil proton:

$$(B\text{-}4) \qquad (E_3)_{\Theta_3^{max}} = m\left[1 - \frac{M^2 - \mu^2}{2 m E_0}\right]^{-1}$$

and it is given by:

$$(B\text{-}5) \qquad \cos\Theta_3^{max} = \frac{1}{2 m p_1}\left[(M^2-\mu^2)(4 m E_0 - M^2 + \mu^2)\right]^{1/2}$$

One can show that at the maximum angle the following relation holds (in the approximation $\beta_1 \simeq 1$):

$$(B\text{-}6) \qquad p_1 (p_3 \cos\Theta)_{\Theta_3^{max}} \cong (M^2-\mu^2)\left(1 + \frac{M^2-\mu^2}{4 m E_0}\right) \cong M^2 - \mu^2$$

One sees that both $(p_3)_{at\ \Theta^{max}}$ and $\cos\Theta_{3\,max}$, for a fixed value of p_1, increase with M.

Going back to Figs. (A1 and A2) one can see that at the minimum of each curve a width for M of 30 MeV requires a precision in the angle within $\sim 1^0$, while p_1 can range from 0.4 to 1 GeV/c.

We are interested now in transferring a given angular distribution of the recoil proton from the C.M. system to the laboratory system. We need simply the Jacobian of the transformation, which can be written, by use of the Lorentz transformations, in the following way:

$$(B\text{-}7)\qquad J\left(p_3, p_3^0, \cos\Theta_3^0\right) = \frac{d\cos\Theta_3^0}{d\cos\Theta_3} = \frac{1}{\gamma_c}\left(\frac{p_3}{p_3^0}\right)^3\left(1+\frac{\beta_c}{\beta_3^0}\cos\Theta_3^0\right)^{-1}$$

where subscript 0 indicates C.M. quantities, and $\beta_c = \frac{p_1}{E_0}$ is the velocity of the C.M. with respect to the laboratory.

Spikes in the angular distribution at Θ^{max}

It is instructive to rewrite the Jacobian in a different way:

$$(B\text{-}8)\qquad J(p_3, p_3^0) = \frac{(p_3)^3}{p_3^0\sqrt{2mE_0}}\left[E_3\left(1-\frac{M^2-\mu^2}{2mE_0}\right)-m\right]^{-1}$$

The two relations (B7), (B8) are easily identified by making use of the Lorentz transformation and the relation (B3).

We see at once that J goes to infinity at the value of E_3 given by (4), which corresponds to the maximum angle Θ_{max}.

The occurrence of this pole can be understood by observing that J represents the angular distribution in the laboratory system corresponding to an isotropic distribution in the C.M. We remark that a pole in the physical region, corresponding to a maximum angle $\Theta^{max} < \pi$, can be present only for $M > \mu$. For $M < \mu$ the expression in brackets (B-8) never vanishes and all the angles are permitted in the laboratory system. ($M = \mu$ represents the limiting case, in which $J \to \infty$ at $\Theta = \frac{\pi}{2}$). The situation in the case $M > \mu$ is represented in Fig. (B-5), where the transformation of the velocity and angle from the C.M. to the laboratory system is given (for the sake of simplicity, non-relativistic composition of velocity is used).

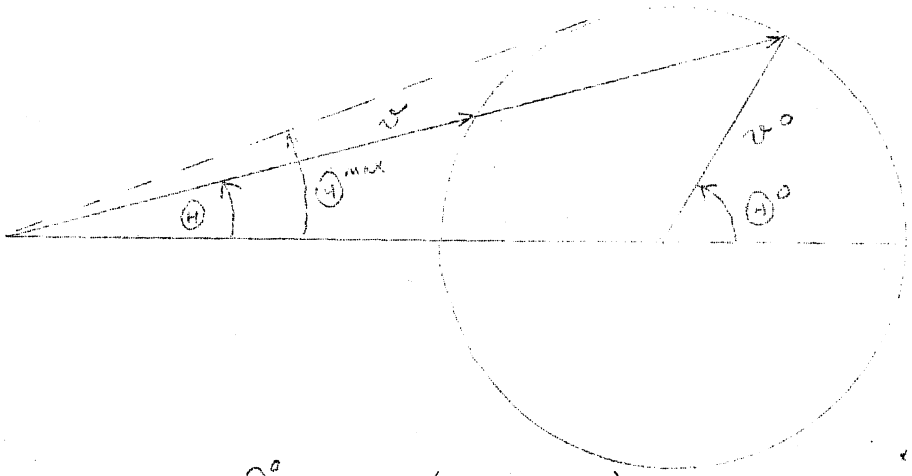

Fig. B-6

We see that, while θ^{o} increases (in the C.M.) from zero to π the laboratory angle θ first increases from 0 to θ_{max} and then decreases to zero. At $\theta = \theta_{max}$ the rate of increase is zero, i.e. $d\cos\theta / d\cos\theta^{o} = 0$.

By means of (B-8) we have transformed the "peripheral" angular distribution evaluated in the C.M. system (with the π, η, and ζ exchanges) to the laboratory system. The infinity at θ_{max} remains in all these distributions. Of course, the integral over a finite range of θ close to θ_{max} is finite.

We give in Figs. (B3, B4 B5) the angular distributions $\sigma(\theta)$ for the different cases (exchange of π, η, ζ). For practical reasons, we have replaced the actual values $\sigma\Theta$ in a small range $\Delta\theta$ close to θ_{max}, with the average value:

$$\overline{\sigma}(\Delta\theta) = \frac{1}{\Delta\theta} \int_{\theta^{max} - \Delta\theta}^{\theta^{max}} \sigma(\theta)\, d\theta$$

Then, one can get easily the relative intensity of the scattered proton in the interval $\Delta\theta$. This, however, is correct only in the case of zero width for M. For a finite width Γ, one has to take into account that the maximum angle θ_{CM} increases (decreases) in going from M to $M \mp \Gamma$ by a certain amount $\Delta\theta_{CM}$. One should add to the intensity in the interval $\Delta\theta$, the one corresponding to the interval $\Delta\theta_{CM}$. This is equivalent to take the averaged sum of different curves, which are obtained by displacing the original distribution

$\sigma(\Theta)$ (corresponding to the value M) along the Θ axis of small quantities increasing from zero to $\Delta\Theta_{CM}$. The curves given in Figs. (B3, B4, B5) are obtained simplifying this procedure by a graphical method.

Further discussion of these distributions is in Appendix C.

APPENDIX C

Dynamics of the Reaction $\pi + P \rightarrow P + X$

In the evaluation of the angular distribution of the recoil proton in the laboratory system, we have assumed a specific hypothesis, namely a peripheral interaction for the production process.

We have considered different possibilities, that is the exchange of a pseudoscalar particle (π and η), and of a vector particle (ρ, ω). Going from the pion mass to the ρ mass, we can cover different degrees of "peripherism".

Since we are interested only in the distributions of the recoil proton, we keep in the production cross section only those terms which depend on the (squared) momentum transfer $\Delta^2 = (p_3 - p_2)^2$. We can write

$$\Delta^2 = 2m\, T_3 \tag{C-1}$$

where T_3 is the kinetic energy of the recoil proton in the laboratory system.

For the exchange of a pseudoscalar particle we have:

$$\frac{d\sigma}{d\Delta^2} \sim \frac{\Delta^2}{(\Delta^2+\mu_{PS}^2)^2} \tag{C-2}$$

and for a vector particle (neglecting the tensor coupling - which is proportional to the momentum transfer; in fact, we are interested in low values of the momentum transfer):

$$\frac{d\sigma}{d\Delta^2} = \frac{(P_1^2+2mE_1)(P_1^2+2mE_1-M^2+\mu^2)-\Delta^2(E_1+2m)E_1}{(\Delta^2+\mu_V^2)^2} \tag{C-3}$$

In the above relations μ_{PS} and μ_V are the mass of the pseudoscalar and vector particle, respectively.

Making use of the relation

$$(C\text{-}4)\quad \Delta^2 = 2\left[(E_2 E_3) - m^2\right] + 2\left[(E_2^2 - m^2)(E_3^2 - m^2)\right]^{1/2} \cos \Theta_3^0$$

where all the quantities refer to the C.M. system, we can easily evaluate from (2), (3) the angular distribution $d\sigma/d\cos\Theta^0$ in the C.M. system. We give the center-of-mass distributions as functions of $\cos \Theta_3^0$ for the cases of π, η and ρ exchanges, for a typical value of p_1 and M (p_1 = 8 GeV/c; M = 2 GeV) in Figures C-1, C-2 and C-3 respectively.

In order to get the angular distribution $d\sigma/d\cos\Theta_3$ in the laboratory system, we have to multiply the above expressions (2) (3) by the factor:

$$(C\text{-}5)\quad \frac{d\Delta^2}{d\cos\Theta} = \frac{4m\, p_1 p_3^3}{2m E_0 (E_3 - m) - E_3 (M^2 - \mu^2)}$$

It is this factor that introduces the Jacobian peaks in the angular distributions at the maximum laboratory angle. The laboratory angular distributions for π, η and ρ exchange are given in App. B, Figures B3, B4 and B5 respectively.

It is seen that neither in the CM nor in the laboratory distributions the differences in the shape between the π and η-exchange mechanisms are experimentally detectable. Even the quantitative differences are negligible: for the π-exchange, the fraction of the events in the Jacobian peak is 17% while for the ρ-exchange it is 23%. However, for the η-exchange, the same figure is 6% and also there is a marked difference in the shape of the distribution, both in the CM and in the laboratory.

We wish to point out that for the pseudoscalar exchange (π and η) the distributions are valid regardless of the spin-parity of the produced particle X. For the exchange of the vector meson, the X is assumed to be pseudoscalar. Since we expect the X to be something like $J = 2^-$ or $J = 3^-$ (tensors) or similar, our calculated distributions for the ρ-exchange are not to be taken too seriously.

Appendix D

Vertex chamber *

The purpose of the "vertex chamber" is to determine the number of charged pions, $\bar{N}\pi$, emitted from the pion-proton vertex. Since we intend to measure $\bar{N}\pi$ only for the events corresponding to peak, if such is found, the vertex chamber should determine the number of charged decay products of X-Meson.

If X also decays into K-mesons, the V's would be expected to be seen a fraction of time.

Physics information we hope to obtain

It has been shown recently by Koba et al **, on the basis of the generalized angular momenta plus iso-spin considerations, that when the following parameters of a boson are given

1) Mass

2) J^P

3) I

the average number of charged pions into which it decays $\bar{N}\pi$, can be calculated.* We recall that our experiment should yield the following set of informations:

1) Mass M_x

2) $I_x \geq 1$

3) $\bar{N}\pi$ (vertex chamber)

4) upper limit on Γ_x

5) differential cross-section $d\sigma_{x/d\omega}$ at the angle Θ^{max} .

---

* Prepared with the aid of G. Charpak

**See e.g. Koba and Grynberg, Physics Letters 1, 34 (1962) and Proc. 1962 Int. Conf. High Energy Physics at CERN, p.178.

It is felt that the above set of experimental information could serve as a base for a speculative spin-parity assignment of the X-meson. While with certainty it could be stated only that informations 1 - 5 will be useful, in favourable cases they may be sufficient for the spin-parity assignment.

Discharge halogene chamber

We propose the discharge halogene chamber to be used as the vertex chamber. Properties of this instrument are listed in Table D-1.

Table D-1

Properties of discharge halogene chamber

	Chamber I (in magn.field)	Chamber II (no magn.field)
Size width x depth z } toward target length y	50 cm 40 cm 50 cm	100 cm 40 cm 50 cm
Filling	Helium + 10^{-4} Iodine	Same as I
Sensitive time	0.5 μs	Not tested but expected same as Chamber I
Recycling period	~ 1 ms	"
Efficiency for minimum ionizing tracks	100%, tested with 15 tracks/picture	"
Max. particle momentum that can be measured to 10% and 20% with H = 16 KGauss	~ 5 GeV/c to 10% ~10 GeV/c to 20%	" "
Max. particle momentum with which the charge can be established. H = 16 KG	~15 GeV/c	"
Special reconstruction of the particle direction	Only two-dimensional reconstruction in x-y plane. Sufficient to the purpose of this experiment.	

Vertex chamber procedure

First procedure:

- The chamber is triggered and the picture taken every time the proton chambers S_1 - S_3 are triggered. The event number appears in the vertex chamber pictures.
- if a peak in the MM-spectrum is found, the event numbers within the peak are listed.
- then, the vertex pictures, with the event numbers corresponding to the peak events are scanned.
- The scanning consists of counting the number of charged prongs and V's.
- the same procedure is done with a comparable number of events outside the peak (= background sample).
- If there is a difference in the average number of charged prongs and V's between the peak events and the background sample, this should be due to the decay properties of the X-meson.

Next procedure:

- The direction of all tracks from the peak events is measured to see if they originate at the Π - P vertex (by means of a programme).
- all tracks that satisfy the vertex condition are counted and $\bar{N}_\pi$ is determined.

We are considering two possibilities:

Small chamber in magnetic field

The existing discharge chamber of volume 50 x 50 x 40 cm^3 placed in the magnetic field of 16 KGauss. The chamber has been tested

in the magnetic field and it is concluded that up to 15 GeV/c particles have a sufficient curvature to establish the particles charge. At this stage, no momentum measurements are planned or needed in the vertex chamber.

The disadvantage of the (small) halogene chamber in the magnetic field is that it will cover an angle of 20° while the maximum angle of the X-decay into 5 bodies is 40° at p_1 = 6 GeV/c. At higher p_1, this angle decreases. The average angle at 6 GeV/c is 20°, so that approximately 50% of the decay products will be lost. The actual number of decay products can be obtained only by applying large corrections, involving both the phase space and the decay properties assumptions.

Large chamber, no magnetic field

A large discharge chamber, without magnetic field. Since, in principle, the size of the chamber is unlimited, it can be made even larger than the one under construction, which is 100 x 40 x 50 cm^3. In this case 90% of the decay products will be observed in the chamber. Charge of each individual decay product will not be determined in this case. The requirement that the number of charged tracks be odd is sufficient to determine the total number of charged decay products.

Figure 1

M_1 , M_2 = magnets

H_1 , H_2 , H_3 = counter hodoscopes

T = liquid hydrogen target

S_1 = thin plate, 5 gap spark chamber, photographic and sonic

S_2 = " " , 3 " " " , " " "

S_3 = " " , 5 " " " , " " "

R1 = Aluminium block, 2.5 cm thick

R2 = " " , 50 cm "

P_1 - P_6 = Scintillation counters

$\bar{P}_1$ - $\bar{P}_3$ = " " in anticoincidence with P_1 - P_6

V = vertex chamber

C = centre plane of M_1 - M_2 spectrometer

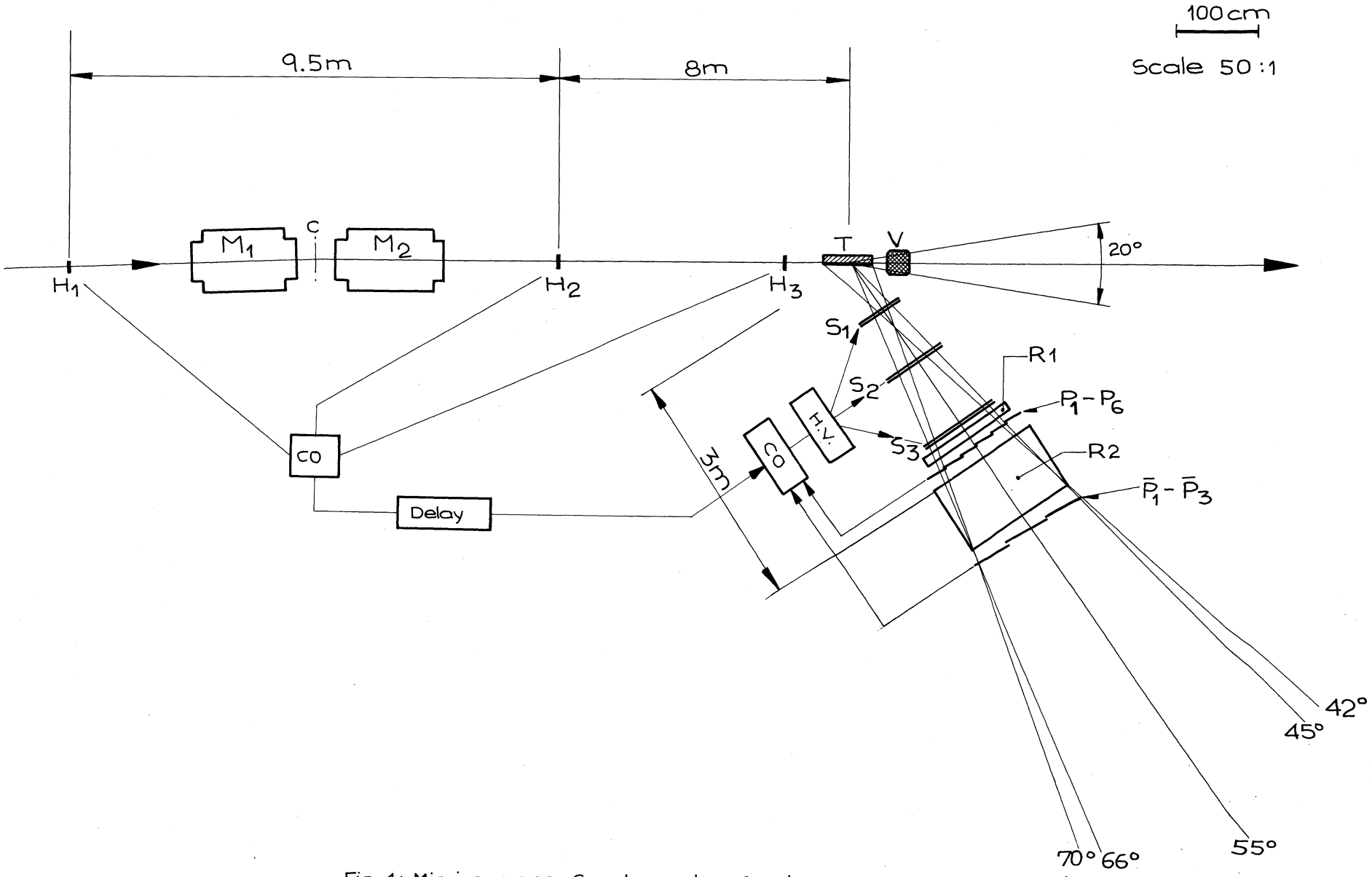

Fig. 1: Missing-mass Spectrometer for heavy Mesons
(Data reduction diagrams are in Figs. 2 and 3)

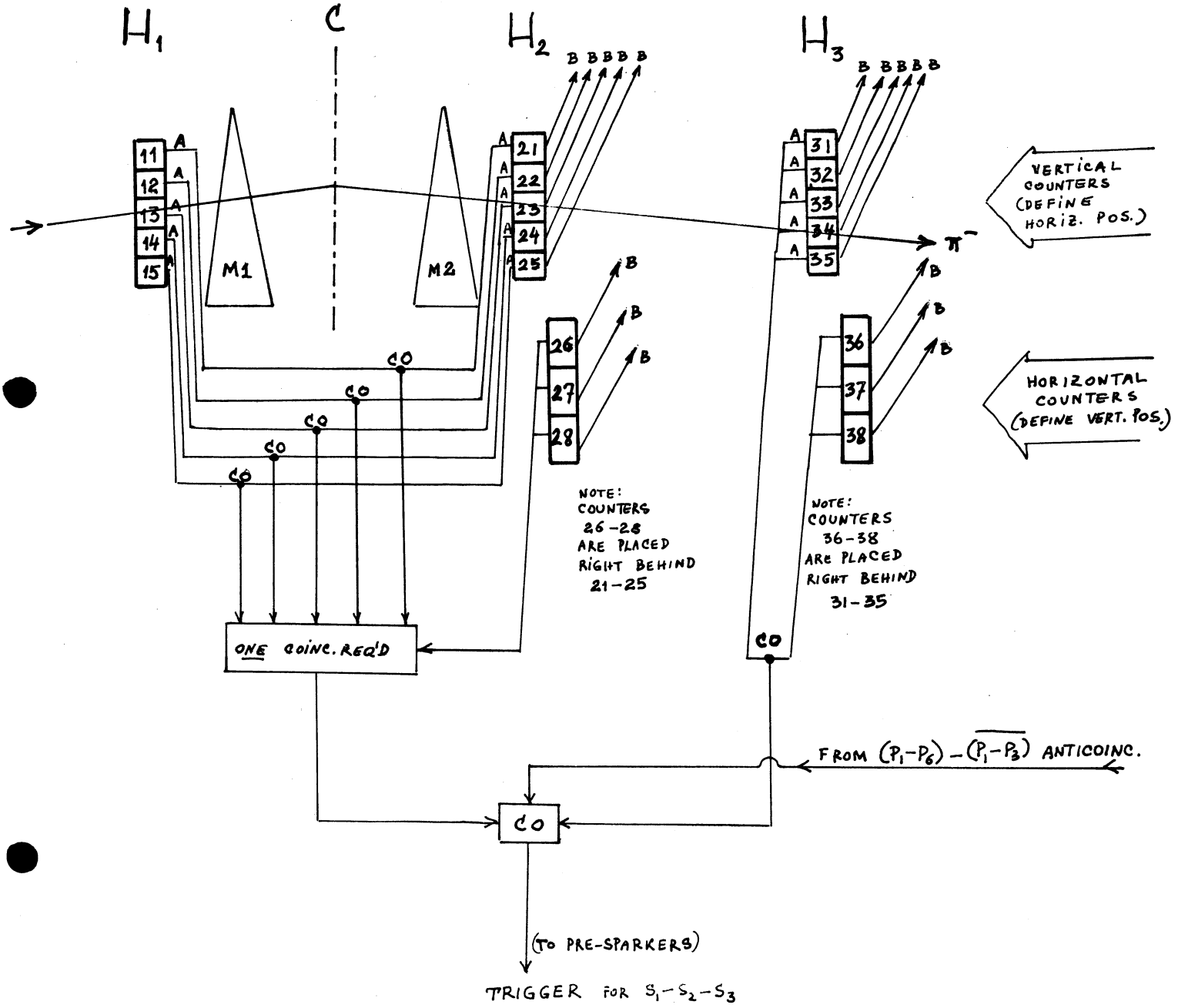

FIGURE 2 BEAM HODOSCOPE CONNECTIONS AND TRIGGER REQUIREMENTS. OUTPUTS "B" GO TO DATA RECORDING SYSTEM

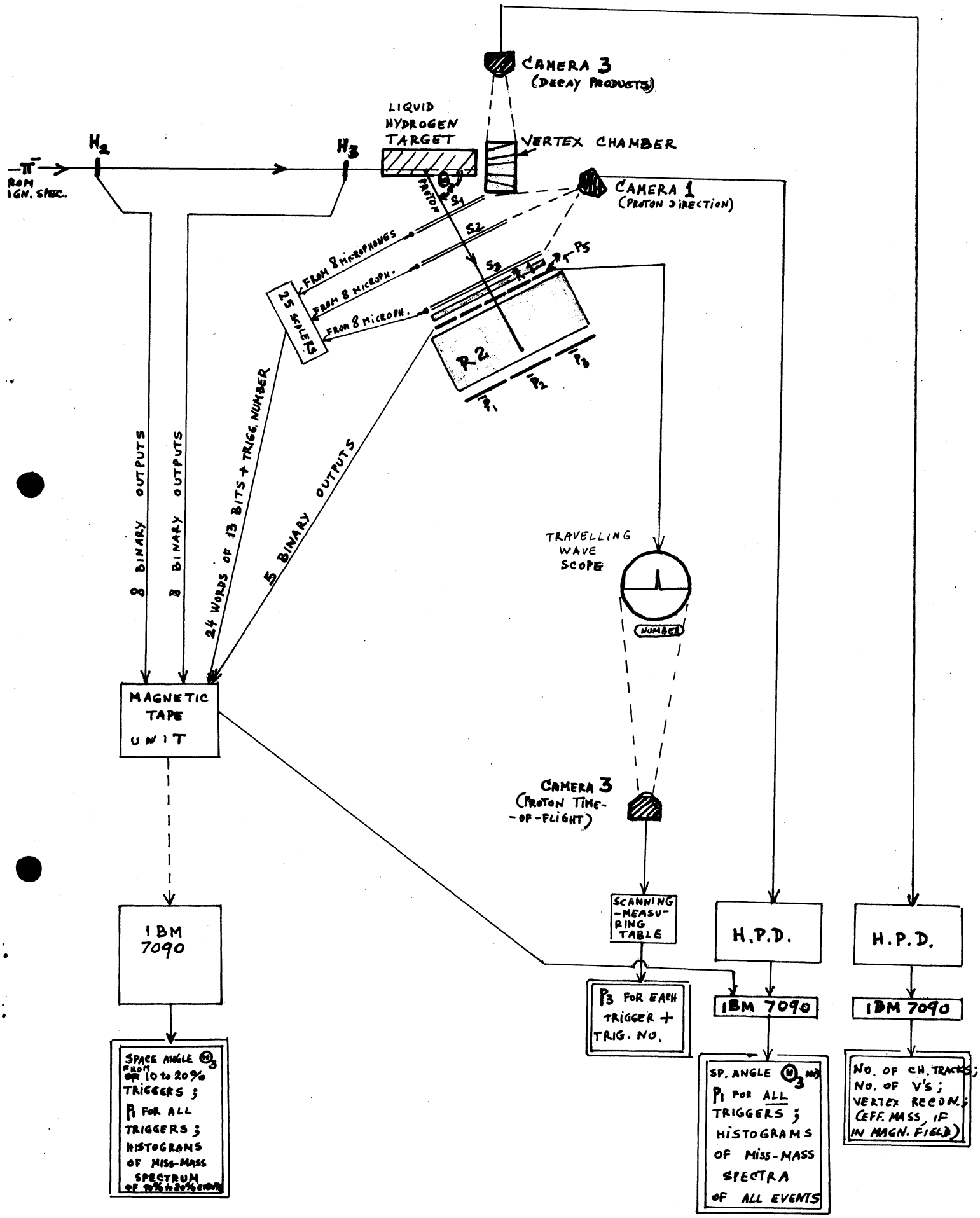

FIGURE 3: DATA REDUCTION SCHEME FOR MM-SPECTROMETER

Figure A1 Mass spectrum of known mesonic states. The area under the curves is proportional to the production cross-section in pion-nucleon collision in the region 1-3 GeV/c. We use the meson spectroscopy notation: J_I^{PG}, where J = spin, I = Isospin, P = parity and G = G-conjugation parity.

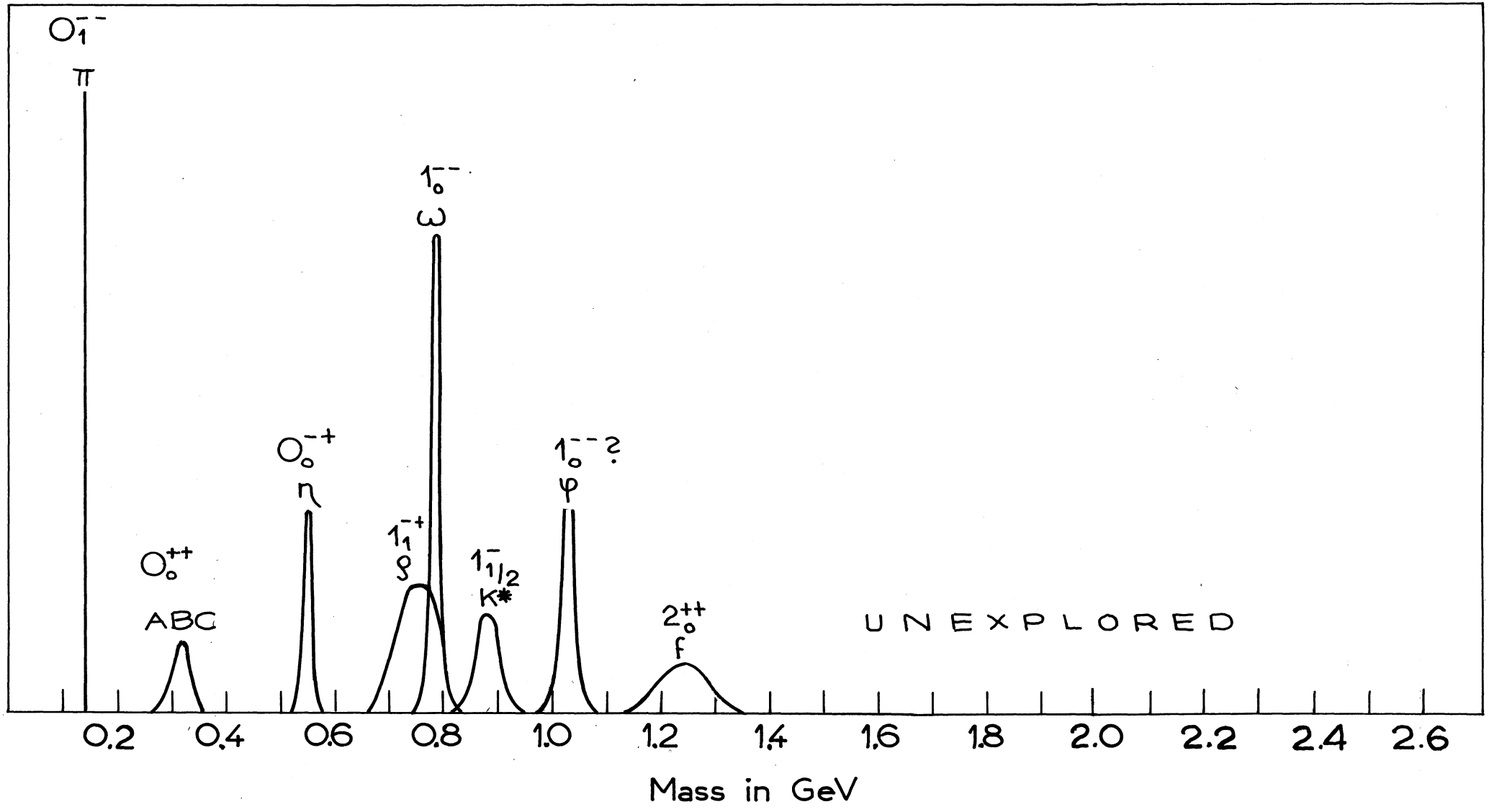
0_1^{--}
π
1_o^{--}
ω
0_o^{-+}
η
1_1^{-+}
ρ
$1_{1/2}^{-}$
K*
1_o^{--} ?
φ
0_o^{++}
ABC
2_o^{++}
f
UNEXPLORED
0.2
0.4
0.6
0.8
1.0
1.2
1.4
1.6
1.8
2.0
2.2
2.4
2.6
Mass in GeV

Fig. A-1

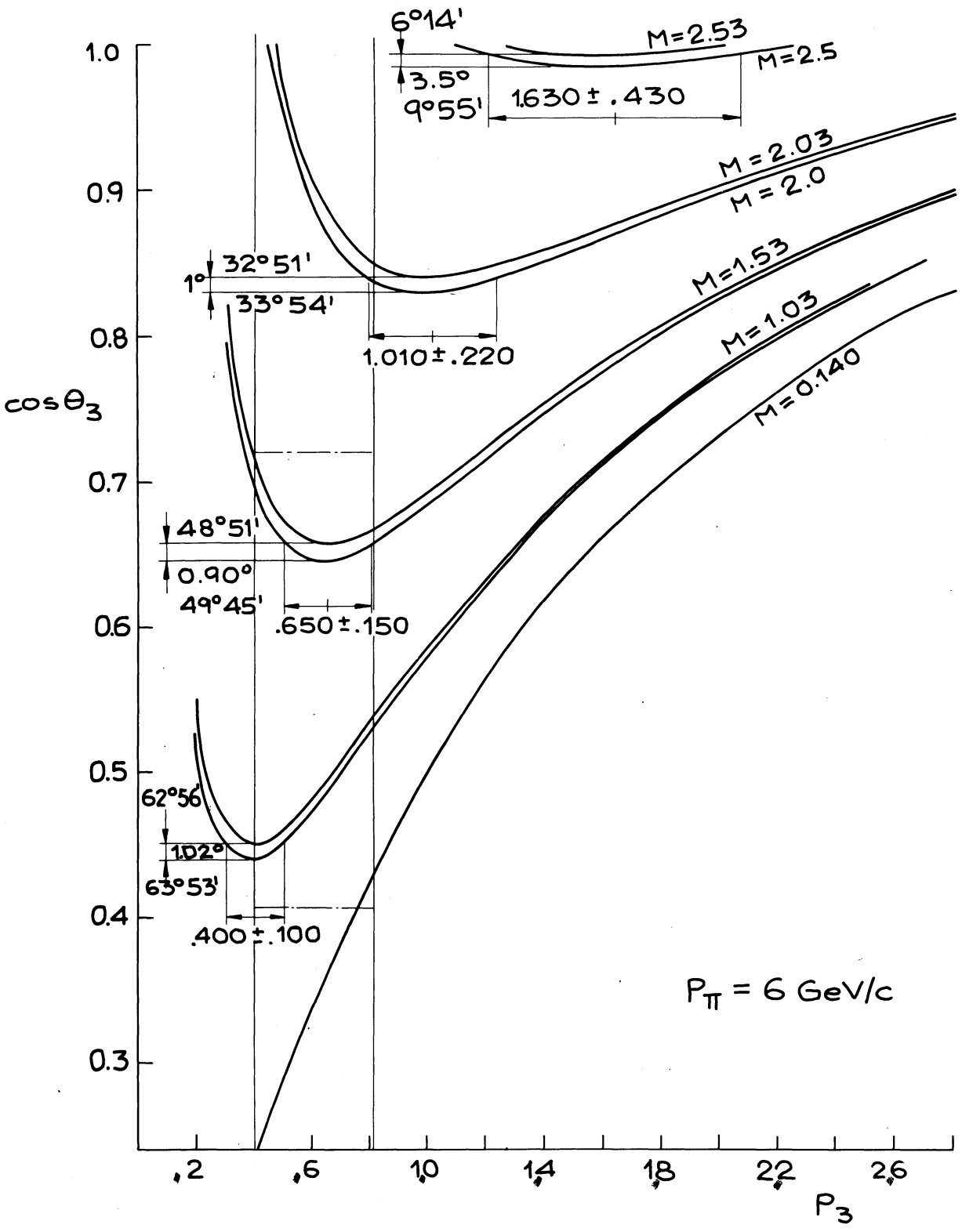
6°14'
M=2.53
M=2.5
3.5°
9°55'
1.630 ± .430
M=2.03
M=2.0
32°51'
1°
33°54'
1.010 ± .220
M=1.53
M=1.03
M=0.140
48°51'
0.90°
49°45'
.650 ± .150
62°56'
1.02°
63°53'
.400 ± .100
P_π = 6 GeV/c
cos θ_3
1.0
0.9
0.8
0.7
0.6
0.5
0.4
0.3
.2
.6
1.0
1.4
1.8
2.2
2.6
P_3

Fig. B-1

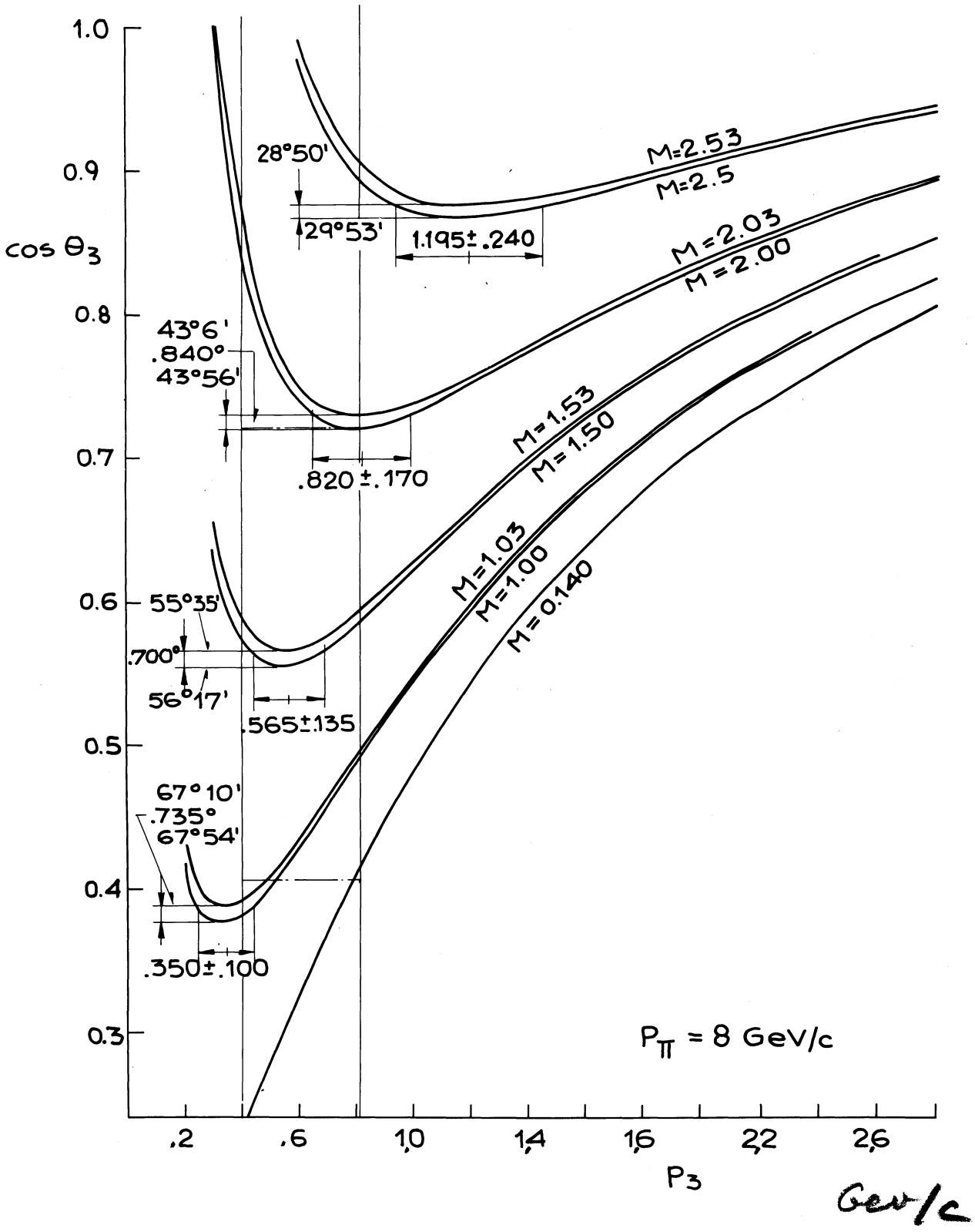
1.0
0.9
0.8
0.7
0.6
0.5
0.4
0.3
cos θ3
28°50'
29°53'
1.195±.240
M=2.53
M=2.5
M=2.03
M=2.00
43°6'
.840°
43°56'
.820±.170
M=1.53
M=1.50
M=1.03
M=1.00
M=0.140
55°35'
.700°
56°17'
.565±.135
67°10'
.735°
67°54'
.350±.100
PT = 8 GeV/c
.2
.6
1.0
1.4
1.6
2.2
2.6
P3
Gev/c

Fig. B-2

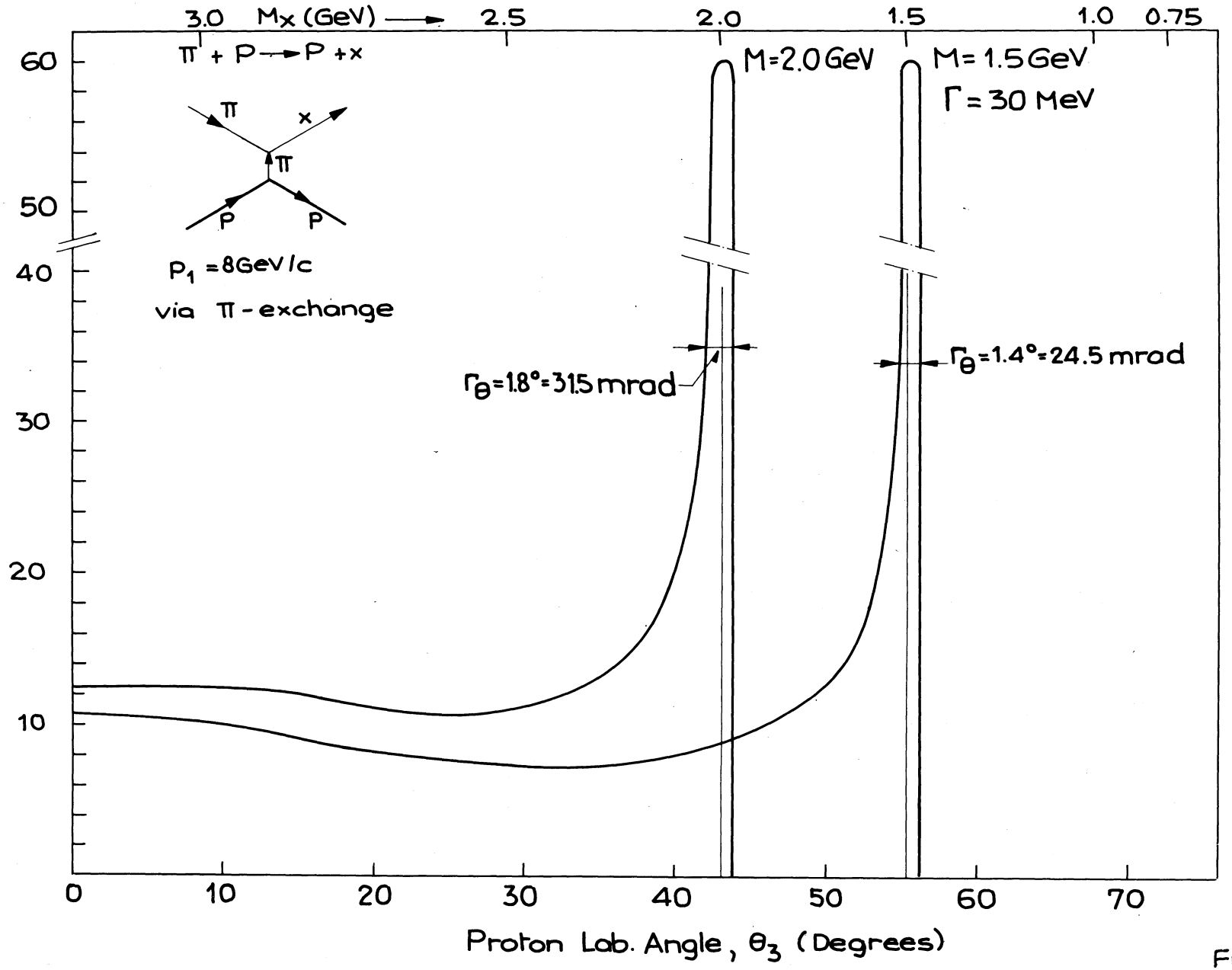

Fig. B-3

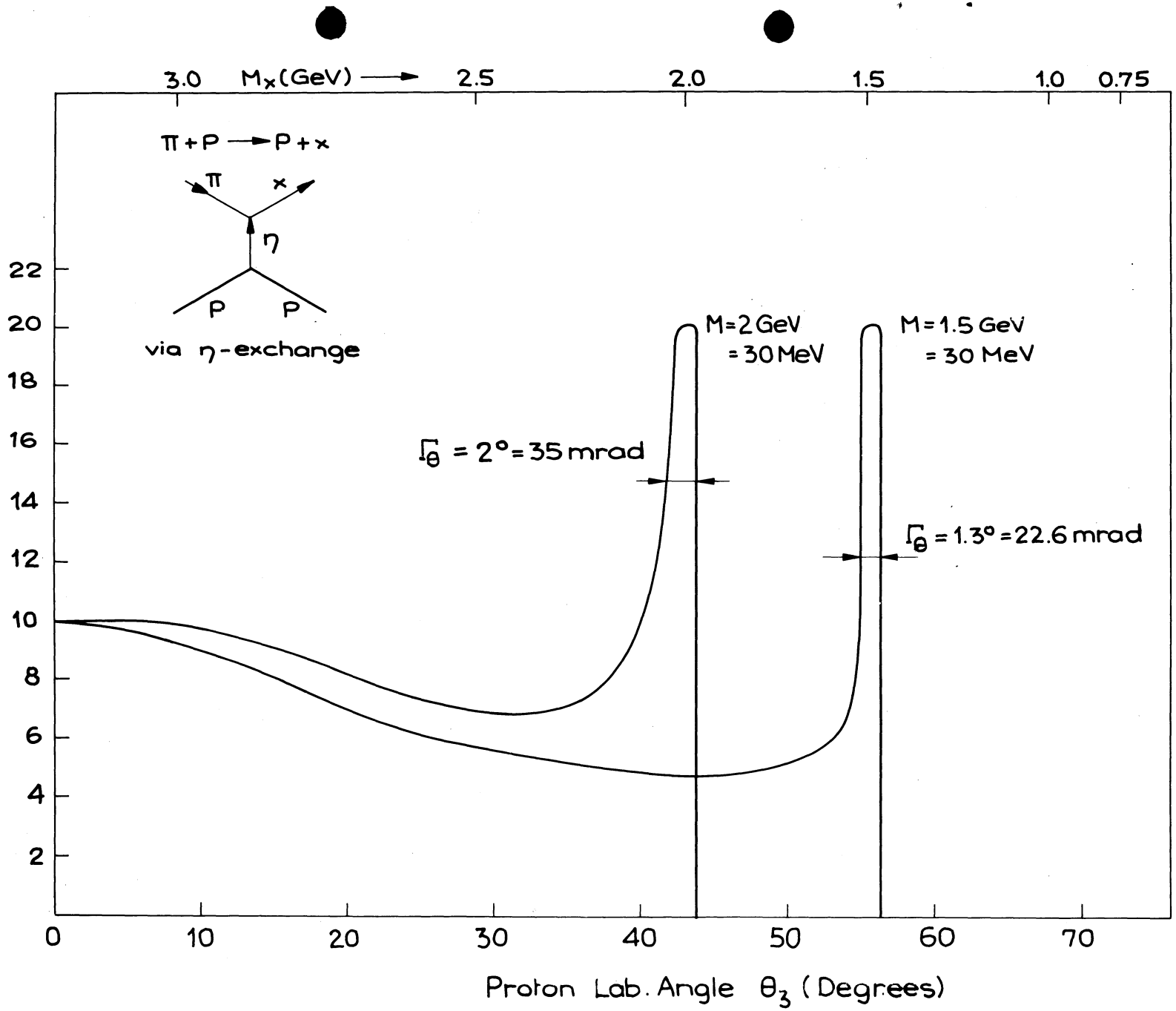
3.0 Mx(GeV) → 2.5 2.0 1.5 1.0 0.75
π + P → P + x
π
x
η
P
P
via η-exchange
M=2 GeV
= 30 MeV
M=1.5 GeV
= 30 MeV
Γθ = 2° = 35 mrad
Γθ = 1.3° = 22.6 mrad
22
20
18
16
14
12
10
8
6
4
2
0
10
20
30
40
50
60
70
Proton Lab. Angle θ3 (Degrees)

Fig. B-4

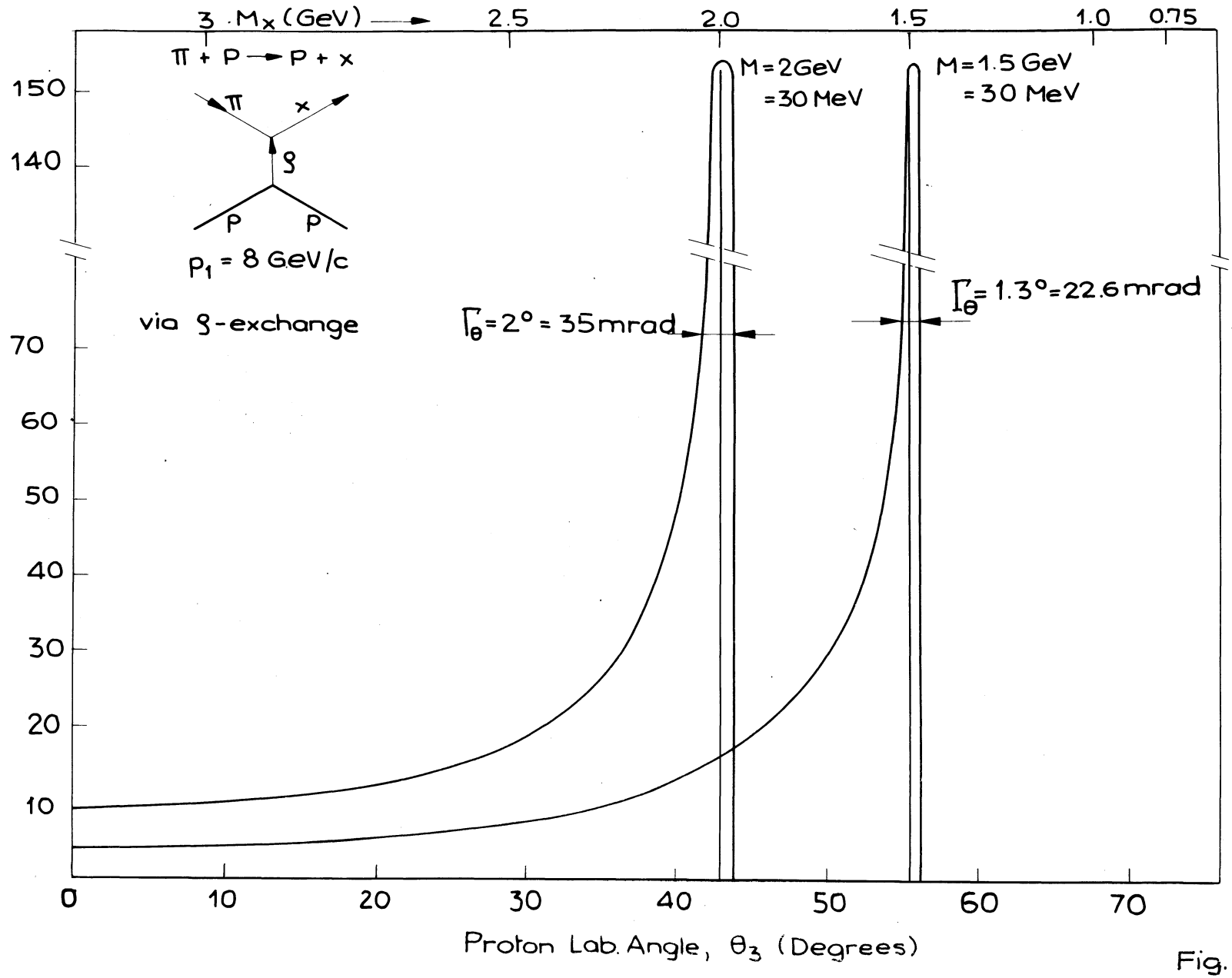

Fig. B-5

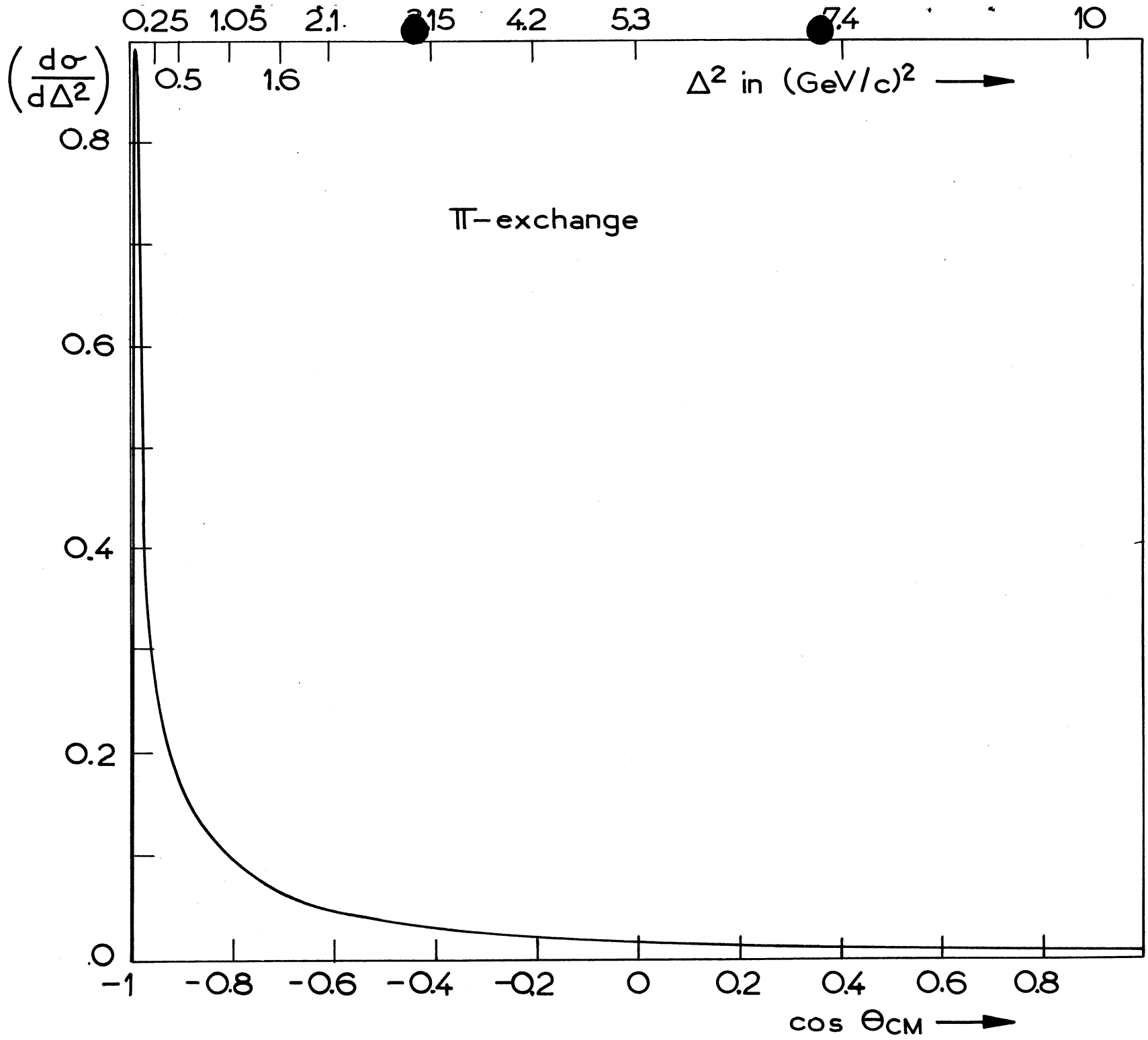
0.25
1.05
2.1
3.15
4.2
5.3
7.4
10
0.5
1.6
Δ^2 in (GeV/c)^2 →
$\left(\frac{d\sigma}{d\Delta^2}\right)$
0.8
0.6
0.4
0.2
0
π−exchange
−1
−0.8
−0.6
−0.4
−0.2
0
0.2
0.4
0.6
0.8
cos θ_{CM} →

Fig. C-1

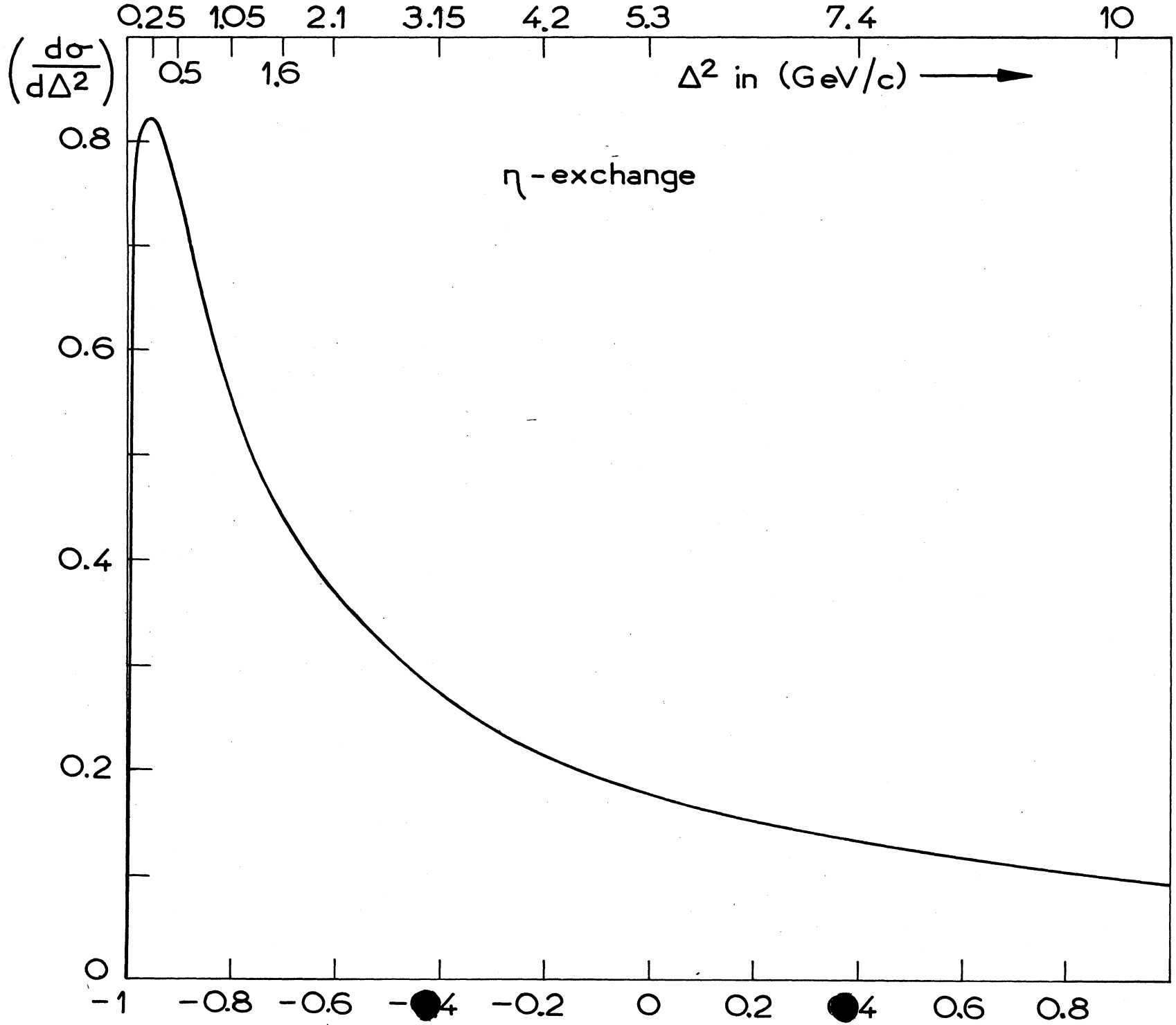
0.25
1.05
2.1
3.15
4.2
5.3
7.4
10
0.5
1.6
Δ^2 in (GeV/c)
$\left(\frac{d\sigma}{d\Delta^2}\right)$
0.8
0.6
0.4
0.2
0
η - exchange
−1
−0.8
−0.6
−0.4
−0.2
0
0.2
0.4
0.6
0.8

SIS/R/6259

SIS/R/6262

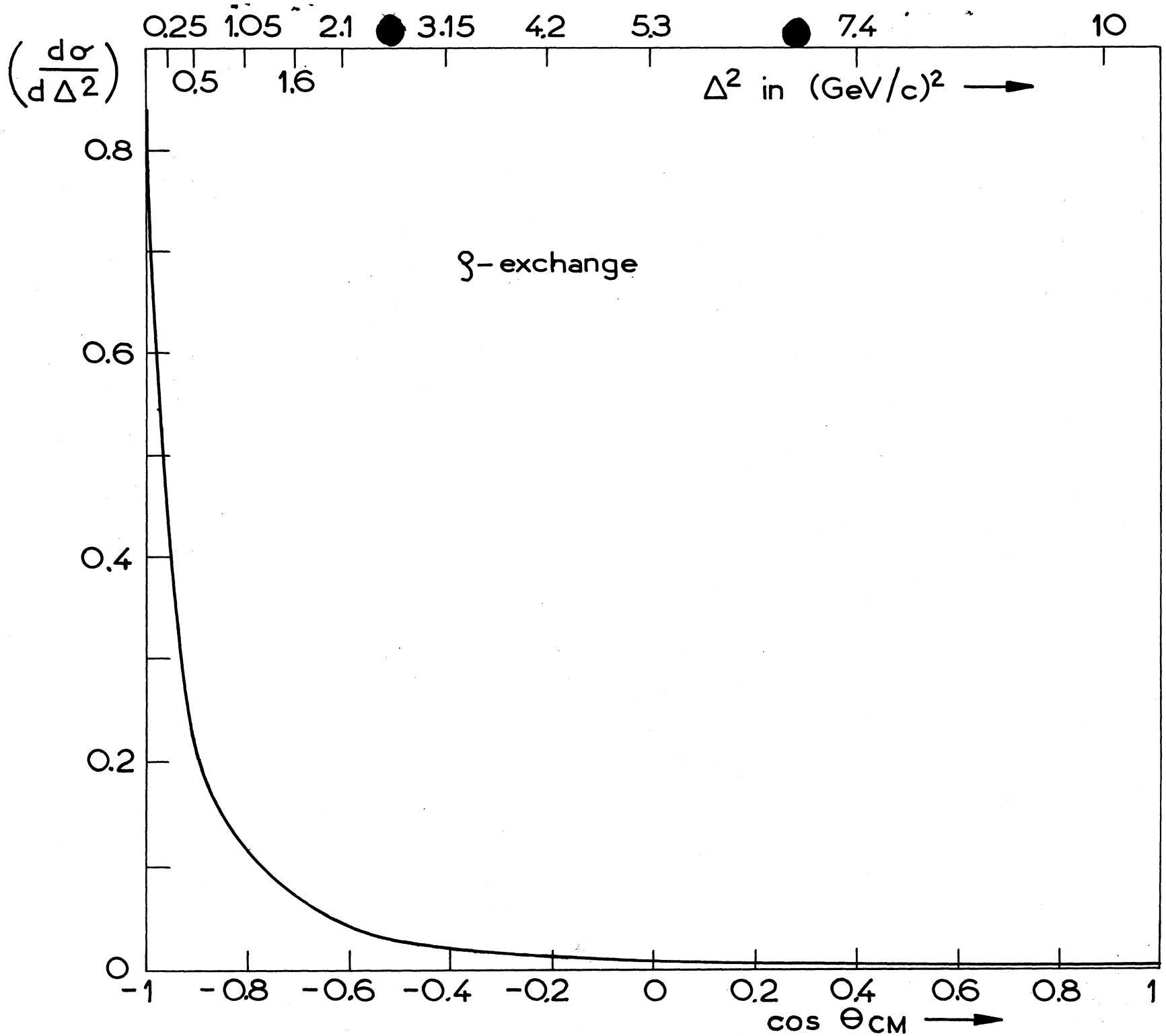

Fig C-3